On the development of an innovative adsorber plate heat exchanger for adsorption heat transformation processes; an experimental and numerical study

Makram Mikhaeil [a], Matthias Gaderer [b], Belal Dawoud [a, *]

[a] Laboratory of Sorption Processes, Faculty of Mechanical Engineering, East Bavarian Technical University of Applied Sciences (OTH-Regensburg), Galgenberg Street 30, 93053, Regensburg, Germany
[b] TUM Campus Straubing for Biotechnology and Sustainability, Chair Regenerative Energy Systems, Technical University of Munich, Schulgasse 16, 94315, Straubing, Germany

ARTICLE INFO

ABSTRACT

An innovative adsorber plate heat exchanger (APHE), which is developed for application in adsorption heat pumps, chillers and thermal energy storage systems, is introduced. A test frame has been constructed as a representative segment of the introduced APHE for applying loose grains of AQSOA-Z02. Adsorption kinetic measurements have been carried out in a volumetric large-temperature-jump setup under typical operating conditions of adsorption processes. A transient 2-D model is developed for the tested sample inside the setup. The measured temporal uptake variations with time have been fed to the model, through which a micro-pore diffusion coefficient at infinite temperature of 2 E−4 $[m^2 s^{-1}]$ and an activation energy of 42.1 $[kJ\ mol^{-1}]$ have been estimated. A 3-D model is developed to simulate the combined heat and mass transfer inside the APHE and implemented in a commercial software. Comparing the obtained results with the literature values for an extruded aluminium adsorber heat exchanger coated with a 500 μm layer of the same adsorbent, the differential water uptake obtained after 300 s of adsorption (8.2 g/100 g) implies a sound enhancement of 310%. This result proves the great potential of the introduced APHE to remarkably enhance the performance of adsorption heat transformation appliances.

1. Introduction

The world loses about 72% of its primary energy in the different energy conversion processes [1]. Most of this lost energy (~63%) is classified as low-grade waste heat (<100 °C), which is quite inefficient to be utilized in electricity generation. Recently, the interest in exploiting such low-grade waste heat as well as solar thermal energy for space heating and cooling has increased considerably. The thermally driven adsorption-based systems have the merit of compatibility with low-grade heat sources [2−4]. However, the low system performance in terms of the coefficient of performance (COP) and the specific power output (SP) together with the high corrosion potential if made partially or totally of aluminium or copper stand as barriers against wide-scale adoption of such

technology for heating and cooling purposes.

Beside the thermal management of the system [5−7] and the development of novel adsorbents [8−17] to enhance the adsorption characteristics of the applied working pair, i.e. the adsorption capacity and the heat of adsorption, the heat exchanger to adsorbent heat capacity ratio represents the most influencing factor on the coefficient of performance (COP) of adsorption heat transformers (AHT) [18]. For a certain amount of adsorbent, the lower the mass of the heat exchanger, including the mass of heat transfer fluid (HTF), the higher the COP of the AHT. The smaller heat capacity of the heat exchanger implies less sensible heat to be consumed in the successive cooling and heating processes, during the adsorption and desorption processes, respectively [18,19].

Beside low cost, manufacturability including a reasonable quality assurance procedure, the dynamic performance design requirements of an effective adsorber heat exchanger include:

a) High overall heat transfer coefficient between the heat transfer medium and the adsorbent.
b) High overall (inter- and intra-particle) mass diffusion coefficient.

Indeed, the kinetics of the adsorption and desorption processes are decisive for the SP. Poor heat and mass transfer characteristics during adsorption and desorption processes lead to longer process times [19–21] and, consequently, lower SP. The heat transfer characteristics of the adsorber heat exchanger may be enhanced by providing large heat transfer surface area per unit adsorbent mass. Aristov et al. [22], investigated the relation between the adsorption kinetics and the ratio (S/m), which refers to the heat transfer surface area to the adsorbent dry mass. The study concluded that the ratio (S/m) can be used to assess the degree of dynamic perfection of an adsorber heat exchanger, especially in case of applying small adsorbent grains (d < 0.5−0.8 mm). The study did not, however, investigate the influence of the mass transfer resistance against the refrigerant flow through the adsorbent bed, which would be the case with smaller grains or with grains with a high size range, where the inter and intra-particle diffusion resistance do influence the dynamics of the adsorption process significantly. The fin efficiency has not been included in this study to estimate the active heat transfer area (S), which results in a rather big deviation between the measured adsorption dynamics on small-scale samples and representative pieces of adsorber heat exchangers [22].

The mass transfer can be enhanced by decreasing the length of the diffusion paths of the refrigerant through the adsorbent bed. To sum up, a thicker and wider adsorbent bed is unfavourable for a high SP. In addition to the dynamic performance design requirements, the following reliability design requirements of a more effective adsorber heat exchanger are quite essential to guarantee a sustainable product [18]:

1. High stability of the adsorbent against hydrothermal aging.
2. High mechanical stability of the adsorbent against loading, transport and operating conditions.
3. No corrosion potential under loading, transport and operating conditions.
4. No release of inert gases upon repeated adsorption−desorption cycling.

Several communications have addressed the issue of optimizing the thermal management inside the adsorber heat exchanger by coating the sorbent directly to the surface of the HEX, either by in-situ crystallisation [23] or by a binder-based technique [24,25], approaches which are very time-consuming with high production cost. Furthermore, only thin films of the sorbent can be applied to the HEX surface due to mechanical strength and mass transfer limitations (<0.5 mm & <0.1 mm for the binder-based & in-situ crystallisation respectively), restricting the volumetric storage density [26]. Thus, the resulting heat storage density is limited, since the amount of sorbent material per unit of volume is low. Moreover, with the binder-based methodology, the release of non-condensable gases from binder degradation is very likely, which alters the conditions inside the adsorption module, thus reducing the performance [27]. The in-situ crystallisation procedure is rather a complex technology due to high pressure and temperature needed during the synthesis process. Indeed, one of the most obvious problems in the field of AHT lies in the fact that, until now, only commercially available heat exchangers have been applied [28,29], which proved to be either too expensive or not durable.

There have been many attempts in the literature to realize high efficient adsorbers. However, most of them applied finned flat or circular tube heat exchangers due to their relatively large extended heat transfer surface area. The majority introduce numerical studies for optimizing the fin spacing and height. No special care have been taken regarding the construction materials from the corrosion point of view. In addition, the use of extended fins to maximize the heat transfer surface area has very decisive disadvantage, in terms of the high heat transfer resistance, which may take place at the fin-root-surface interface of circular finned-tube heat exchangers, and the related decrease on both COP and SP [30,31]. Brazed finned-flat-tube heat exchangers are made of different aluminium alloys and are, therefore, subjected to corrosion against water, ethanol or methanol under the operating conditions of adsorption heat transformation appliances [18,21and32]. The inert gases released out of such corrosion reactions result in a significant performance reduction and on the long run, in destroying the heat exchangers and, consequently, the whole machines [18,32]. If remarkable progress shall be achieved in this crucial field of science to effectively participate in mitigating the severe global warming consequences, dedicatedly designed heat exchangers must be developed tested and optimized, which fulfils the operational, manufacturing price and durability targets simultaneously [32].

This study aims, therefore, at introducing an innovative adsorber plate heat exchanger (APHE), which has been specially developed for application in AHT appliances [33]. A dedicated test frame have been developed and applied to test the adsorption/ desorption kinetics on a small-scale adsorbent sample of loose grains, which is representative for the loose pellets' arrangement inside the full scale APHE. Furthermore, a 2-D mathematical model is developed to simulate the combined heat and mass transfer encountered in the tested small-scale adsorbent mass in a volumetric LTJ kinetic setup [34,35]. The model has been implemented in COMSOL Multiphsyices® software. Thanks to the optimization module integrated in COMSOL, the mass diffusion parameters of water vapour in AQSOA-Z02 pellets have been estimated by best fitting the simulation results to the experimental data. The estimated parameters for the diffusion coefficient have been utilized to simulate the full scale APHE with a more sophisticated mathematical model, in which the transient coupled heat and mass transfer on the adsorbent/adsorbate, the transient heat transfer on the metal plates and the transient convective heat transfer on the heat transfer fluid (HTF) domain have been considered.

2. The proposed adsorber plate heat exchanger (APHE)

To completely avoid corrosion, the developed APHE [33] has been designed as an open-structured stack of multi-nickel-brazed parallel plate-pairs made of stainless steel 316l, wherein each plate-pair comprises an inlet and an outlet port of 16 mm diameter for the HTF. The dimensions of one plate is 400 mm in length and 54 mm in width. The plate thickness amounts to 0.3 mm. Fig. 1.a depicts the upper part of the APHE showing the exit port for the HTF, which is connected to the inlet port by seven parallel flow channels, each has an internal diameter of 2 mm. The clearance between each two successive plate-pairs in the stack amounts to

3 mm, which shall be filled in with loose adsorbent grains. The stacked plate pairs shall be Nickel-brazed together on the annular rings of the inlet and outlet ports of the HTF to form the APHE. A suitable cage made of two segments of a perforated stainless steel sheet has been developed for the APHE to be mounted inside, in order to prevent the adsorbent grains from falling out of the heat exchanger [33]. Fig. 1. b shows the APHE mounted inside the adsorber/desorber chamber, which shall be connected to the evaporator/condenser chamber via the vapour duct [33]. The APHE shall be mounted inside the adsorber/desorber chamber, which shall be connected to the evaporator/condenser chamber. Fig. 1. c presents the cross section A-A of Fig. 1. a to illustrate the gap between two successive plate pairs, which is open from both sides and shall be filled in with the adsorbent grains. Water vapour can penetrate, therefore, into the adsorbent grains from both sides of the stacked APHE.

The number of the plate-pairs composing the APHE is determined according to the required space volume for the adsorbent material. To provide a space volume of 1 L, the APHE shall consist of 24 plate-pairs.

3. Test frame and experimental work

Fig. 1. c illustrates the cross section A-A of Fig. 1.a of the APHE, which consists of identical plate-pairs. Water vapour, which fills the adsorber/desorber vacuum chamber shall flow from both sides of the stack into the adsorbent porous media filling the gap between each two successive plate-pairs during adsorption phase and leaves also from both sides of the stack during the desorption phase. It is, therefore, why the symmetrical axis B−B does exist for both heat and mass transfer in the middle width of the plates. The second symmetrical axis C−C stays for heat transfer in the middle height of the adsorbent gap between each two successive plate pairs, as the porous media is equally cooled-down or heated-up by the two contacting plate pairs.

Recalling that the sample mass required for a V-LTJ kinetics' setup [34,35] is limited to 250 mg, in order to allow the adsorption or desorption measurements under quasi isobaric (Δp<2 mbar) conditions. In addition, the small-scale adsorbent sample should be in close agreement with the adsorbent bed of the APHE, in terms of the heat and mass transfer paths. Our experimental setup enables exposing the sample to cooling/heating effect from only one side of the sample holder inside the measuring cell. Because of the symmetry of the adsorbent domain in the proposed APHE around the axis C−C, the heat transfer in a small-scale sample with a height equal to half of the adsorbent layer thickness and exposed to cooling/heating effect only from the bottom side shall be in close agreement with the heat transfer pattern in a half-adsorbent layer. The mass transfer symmetry around the axis B−B in Fig. 1. c enables cutting down the length of the adsorbent sample inside the test frame to half of the width of the APHE. Accordingly, the red segment in the lower left corner of Fig. 1. c must be sufficient to represent the heat and mass transfer behaviour of the APHE, provided that, the cooling pattern of the plate pairs is identical with that of the sample holder of the measuring cell, which has been already approved (see Fig. 6).

Knowing the bulk density of dry AQSOA-Z02 pellets, in the tested grain-size's range of 0.61−0.7 mm, the corresponding width of the sample inside the test frame, through which water vapour shall flow is estimated to 11 mm. A dedicated test frame made of polyether ether ketone (PEEK) has been designed and realized by milling (see Fig. 2), in which the adsorbent grain sample shall be placed. The frame has a slot on one side, which allows the water vapour to enter/leave the adsorbent domain through a fine stainless-steel sieve. The frame prevents the vapour to enter/leave
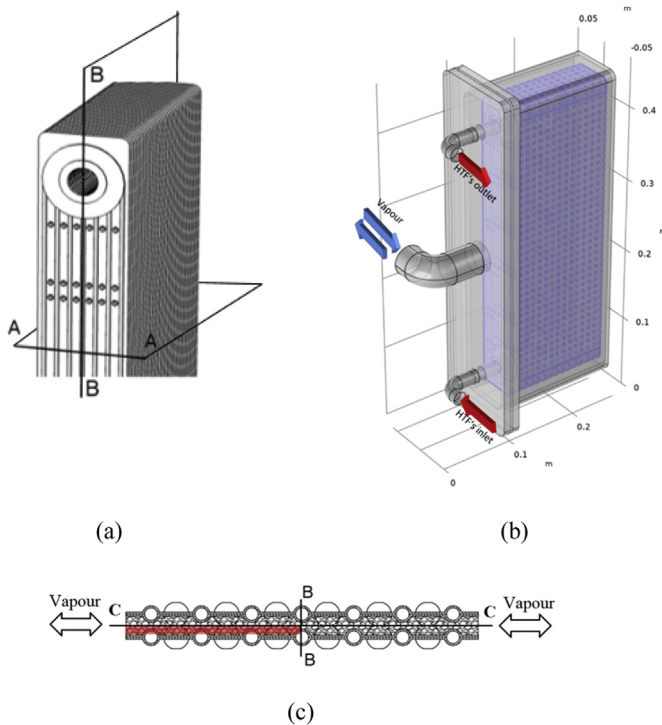

Fig. 1. The developed adsober plate heat exchanger (APHE) [33]; (a) a 3D-Segment showing the top end of the APHE, (b) the APHE inside the adsorber/desorber chamber and (c) a cross section in two successive plate pairs (A-A in Fig. 1a) showing the open structure of the APHE.

(a)   (b)
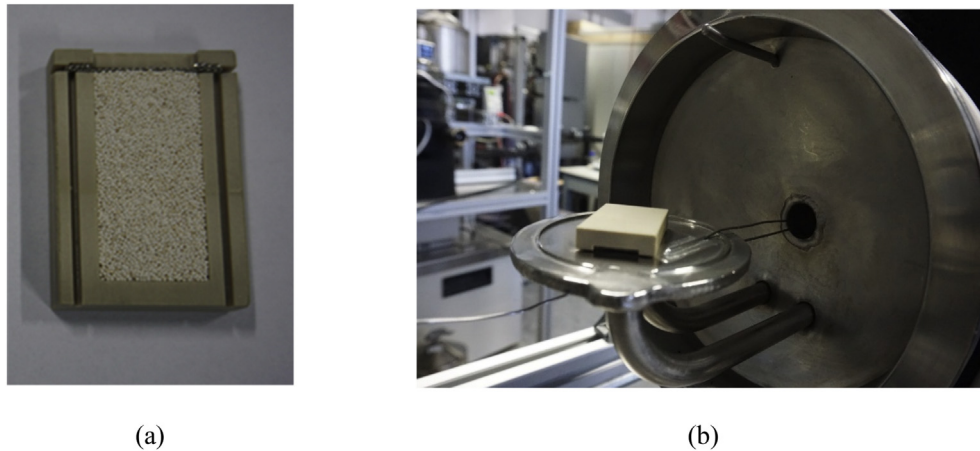
Fig. 2. The frame prepared for testing the adsorption kinetics on a small scale adsorbent sample representing the behaviour of the whole APHE; (a) test frame filled in with loose grains and (b) test frame mounted on the surface of the sample holder of the V-LTJ kinetic setup.

the adsorbent domain from all other sides and allows the heat transfer only from/to the adsorbent mass through a piece of aluminium adhesive tape mounted at the frame's bottom side. The test frame, placed on the sample holder inside the measuring cell of the kinetic setup, is illustrated in Fig. 2. b. The corresponding height of the sample is 1.5 mm, half the thickness of an adsorbent layer in the proposed APHE. The test frame placed on the sample holding surface of the V-LTJ adsorption kinetics setup (Fig. 2b), which is cooled down or heated up during adsorption or desorption processes, respectively, allows realizing heat and mass transfer patterns inside the tested adsorbent sample, which are very close to the patterns occurring in the adsorbent domain of the proposed APHE. Two adsorption kinetic measurements at different evaporator-temperatures 5 and 10 °C have been carried out at adsorption- and desorption-end temperatures of 35 and 90 °C, respectively.

With the help of the available equilibrium data for water vapour adsorption on AQSOA-Z02 zeolite [36], the temperature at which the isobaric adsorption phase of an adsorption heat pump/chiller starts ($T_{ad-start}$) is determined. Thus, to realize water uptake at the beginning of the adsorption processes corresponding to condenser temperature of 35 °C (adsorption-end temperature), driving source temperature of 90 °C (desorption-end temperature), and evaporator temperatures of 5 and 10 °C, $T_{ad-start}$ is determined to 56 and 61 °C, respectively. The details of the V-LTJ kinetic setup, the experimental procedure and the evaluation of the instantaneous water uptake can be read elsewhere [34,35]. Table 1 illustrates the accuracy of the applied individual sensors.

4. Mathematical modelling

The experimental activity carried out in this work on a representative segment of the introduced APHE does require modelling

and simulation work for the subsequent design optimization and upscaling activities.

4.1. Estimation of the mass diffusion parameters

For the mathematical modelling of the APHE, the parameters of the equation governing the diffusion of water vapour on the AQSOA-Z02 grains (linear driving force model) are necessary, namely the mico-pore diffusion coefficient at infinite temperature (D_∞) and the activation energy (E_a). To account for the water vapour diffusion on the AQSOA-Z02 grains, Intini et al. [37], applied the D_∞ and E_a values estimated for the water vapour diffusion in standard zeolite 3 A [38], while Ali and Chakraborty [39] applied the values estimated for the Fuji Davison silica type A [40]. It was reported in Ref. [39] that the effective diffusivity of the water vapour on the AQSOA-Z02 has not been measured before. For a grain diameter of 0.3 mm, Youssef et al. [41], have estimated the diffusion parameters for water vapour adsorption onto AQSOA-Z02 by best fitting the linear driving force model to the obtained isothermal kinetic data by a DVS instrument. They reported for D_∞ and E_a the pairs of 4.85E-9 m^2 s^{-1} and 17709.8 J mol^{-1} as well as 2.77E-5 m^2 s^{-1} and 44423.5 J mol^{-1}, for the pressure ratio (Pr) between the bed (equilibrium pressure) and evaporator heat exchanger (saturation pressure) of >0.1 and $\leq$ 0.1, respectively. Deviations between the measured and predicted temporal water uptake in the range of $\pm15\%$ have been obtained. In Teo et al. [42], D_{so} was implicitly included in the adsorption rate coefficient (K_{ads}), which beside its dependency on both vapour pressure and temperature also depends on the activation energy E_a, which has been estimated to 52,250 J mol^{-1} for AQSOA-Z02.

The first part of the modelling work aims, therefore, at estimating the values of D_∞ and E_a for the water vapour diffusion on the investigated AQSOA-Z02 grains. To this aim, a transient 2-D

Table 1
Sensors applied in the measurements and their accuracies.

Sensor	Accuracy	Measured quantity
Balance KERN type ALS 250-4 A	±0.0007 g	Dry weight of the tested sample
Pressure transducer PFEIFFER VACUUM type CMR 362	±0.2% of reading	Vapour pressure inside the vessel and measuring cell
RTD temperature sensors TMH type Pt100	1/10 DIN class B (±0.1 °C)	Vapour temperature inside the vessel and measuring cell and sample holder surface temperature

(a)   (b)
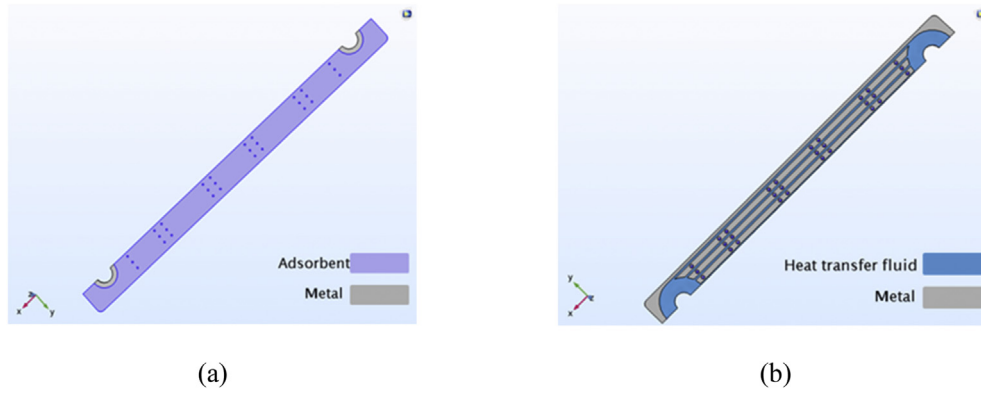
Fig. 3. The intermediate representative segments of the APHE selected for the numerical simulation; (a) adsorbent-metal domain and (b) metal-HTF domain.

mathematical model is developed to simulate the sorption behaviour of the adsorbent sample during quasi-isobaric processes, when the adsorbent sample is subjected to sudden temperature drop. The model accounts for the combined heat and the mass transfer process inside the adsorbent sample. The experimentally recorded values for the instantaneous sample holder surface temperature and vapour pressure inside the measuring cell are fed into the model to account for the time-variant boundary conditions of the sample. By best fitting the model results with the experimental data, the mass diffusion parameters of water vapour in the AQSOA-Z02 grains (D_∞ and E_a) have been estimated.

the HTF domains between the successive plates are identical as well. Therefore, the numerical simulation of only an intermediate section can predict the performance of the whole APHE. Indeed, the adsorbent and HTF domains are symmetric around the axis B–B in Fig. 1. a, which divides it into two equivalent parts. For one representative plate-pair, half of the adsorbent domain thickness on each side, is sufficient to represent the whole APHE. Therefore, a section of the APHE composed of three contacted quarter parts of the domains of the adsorbent, the HTF and a plate-pair (metal) is selected to be the domain of the numerical study (see Fig. 3).

4.2. Modelling of an intermediate section of the APHE

To develop a mathematical model for predicting the performance of the proposed APHE and, at the same time, consumes a reasonable computational time, an appropriate domain for the numerical study should be carefully selected. Since the proposed APHE consists of several identical plate-pairs, the adsorbent and

4.3. Models' assumptions

For both 2-D and 3-D mathematical models, the following assumptions are adopted:

1. The grains in the adsorbent sample are spherical with a uniform size and porosity.
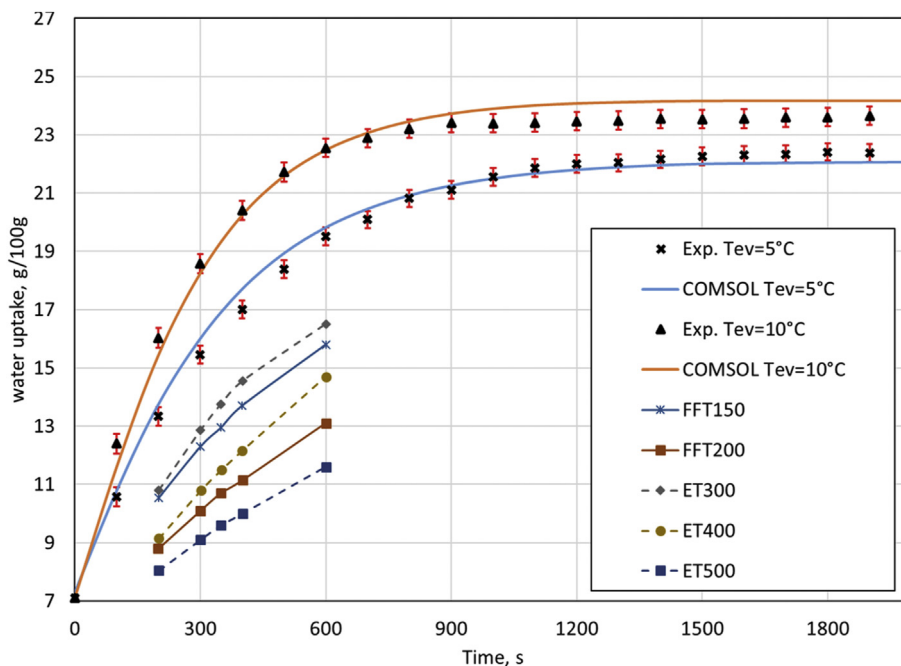
Fig. 4. Experimental and numerical water uptake of the investigated sample at two different evaporator temperatures compared with the adsorption kinetics of two different (FFT: Finned-Flat-Tube & ET: Extruded tube) coated adsorber heat exchangers [21].
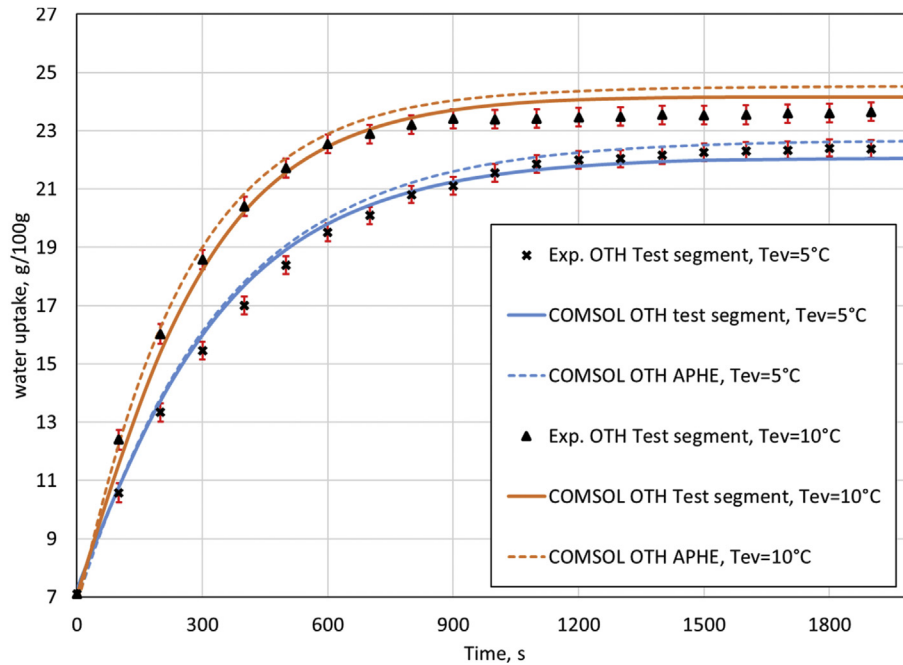
Fig. 5. Experimental and numerical water uptake of the investigated sample compared to the numerical average water uptake obtained from the APHE's simulation at two different evaporator temperatures.
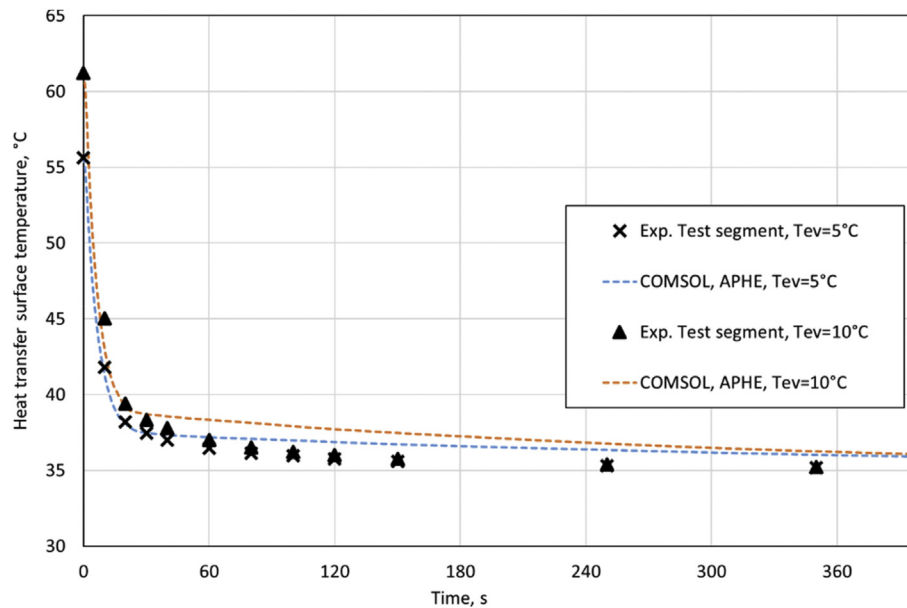
Fig. 6. Experimental sample holder's surface temperature and numerical average temperature of the metal plate's surface at two different evaporator temperatures.

2. Perfect thermal insulation at the upper surface, the side surfaces and the back surface of the adsorbent sample of the 2-D model and the adsorbent domain in the 3-D model.
3. Local thermal equilibrium is assumed between the adsorbent, the adsorbed water and the water vapour.
4. The thermo-physical properties of the dry adsorbent grains are assumed constant.

In addition, the following two assumptions are adopted for the

2-D model of the representative segment of the APHE on the sample holder of the kinetic setup.

a) The temperature distribution over the sample holder of the measuring cell is considered uniform.
b) Water vapour is treated as an ideal gas.

For the 3-D model of the APHE domains, the pressure of the water vapour inside the adsorber chamber is assumed constant and

equals the saturation pressure at the evaporator temperature.

Based on the above assumptions and description of the adsorbent sample inside the kinetic setup along with the selected domains of the APHE, the governing equations described in the following section have been applied.

4.4. Governing equations

As mentioned before, the 2-D mathematical model is specifically developed to account for the combined heat and the mass transfer within the adsorbent sample of the kinetic setup. The sample holder surface temperature is measured continuously during the adsorption and desorption experiments. The sample holder is small and effectively cooled down and heated up, thus assuming a uniform temperature distribution over its surface is quite reasonable. In addition, the sensor used to measure its surface temperature is fixed very close to the position, where the sample is placed (see Fig. 2b). Therefore, the experimentally measured sample holder surface temperature is applied as a thermal boundary condition at the bottom side of the adsorbent sample. Accordingly, the following conservation equations for the heat and mass transfer in the adsorbent sample are adopted.

Energy balance for the adsorbent:

The energy balance for the adsorbent can be described by equation (1) after neglecting the viscous dissipation and the work done by pressure [43].

$$\rho C_{p_{eq}}\frac{\partial T}{\partial t} + \nabla(-k_{eq}\nabla T) + \nabla(\rho_v C_{p_v}\overrightarrow{u_v}\,T) = (1-\varepsilon_t)\rho_{ad}\Delta h_{ad}\frac{\partial w}{\partial t} \qquad (1)$$

Herein, $\rho C_{p_{eq}}$ represents the equivalent heat capacity of the adsorbent bed. The bed can be described as a porous medium of adsorbent grains. The grains contain water in their gas phase as well as in their adsorbate phase. Based on the heat capacity of the adsorbent grains, where the vapour and the adsorbate are co-existing and the heat capacity of the vapour surrounding the grains, the equivalent heat capacity $\rho C_{p_{eq}}$ is determined as follows [43]:

$$\rho C_{p_{eq}} = (1-\varepsilon_t)\rho_{ad}(1+w)C_{ad,\,wet} + \varepsilon_t\rho_v C_{p_v} \qquad (2)$$

The bed total porosity is given by equation (3) in Ref. [44].

$$\varepsilon_t = \varepsilon_b + (1-\varepsilon_b)\,\varepsilon_p \qquad (3)$$

The water vapour is treated as an ideal gas and the vapour density can be calculated as

$$\rho_v = \frac{P}{RT} \qquad (4)$$

The equivelant thermal conductivity of the adsorbent porous medium (k_{eq}) is described by equation (5) [45].

$$k_{eq} = (1-\varepsilon_b)k_{ad,wet} + \varepsilon_b k_v \qquad (5)$$

where $k_{ad,wet}$ is the average thermal conductivity of the wet adsorbent.

Mass balance for the adsorbate:

Equation (6) describes the mass conservation of the adsorbate (water) within the whole system incorporating both adsorbed and the vapour phases [44]. Indeed, water vapour transfers from the vapour phase into the adsorbed phase during adsorption and vice versa during desorption.

$$\varepsilon_t\frac{\partial\rho_v}{\partial t} + \nabla(\rho_v\overrightarrow{u}_v) = -(1-\varepsilon_t)\rho_{ad}\frac{\partial w}{\partial t} \qquad (6)$$

In equation (6), $\frac{\partial w}{\partial t}$ describes the time rate of change of the water uptake per unit mass of dry adsorbent. The intra-particle mass transfer resistance inside the adsorbent grains affects this rate. The well-known linear driving force model [46] is applied to account for such mass transfer resistance as described by equation (7), where D represents the diffusion coefficient, r_p the radius of the adsorbent grains, w^* the equilibrium uptake at the instantaneous pressure and temperature and w the temporal water uptake inside the adsorbent grain.

$$\frac{\partial w}{\partial t} = \frac{15D}{r_p^2}\,(w^* - w) \qquad (7)$$

The equilibrium correlation between pressure, temperature and water uptake for AQSOA-Z02/Water pair is described by the Dubinin-Astakov-Equation (8), where the parameters w_o, E and n have been listed in Ref. [36]. The adsorption potential A is defined by equation (9).

$$w^* = w_o\exp\left(-\left(\frac{A}{E}\right)^n\right) \qquad (8)$$

$$A = RT\,ln\left(\frac{P_{sat}}{P}\right) \qquad (9)$$

Kärger and Ruthven [47] have introduced the following equation (10) to account for the diffusion of a single component into the micro-pores of a porous adsorbent. The micro pore diffusion coefficient D or the "Fickian diffusivity" is thus the product of the self diffusion (mobility) coefficient D_o or the "corrected diffusivity" and the thermodynamic correction factor according to Darken [48]. The Darken factor $\frac{d\ln p}{d\ln w}\big|_T$ is the inverse of the slope of the equilibrium adsorption isotherm of the pure gas. In fact, except in dilute systems, the Fickian diffusivity is generally concentration dependent. Equation (10) shows that this dependence may arise from the concentration dependence of either D_o or $\frac{d\ln p}{d\ln w}\big|_T$. The concentration dependence of the thermodynamic correction factor is found to be much more pronounced than the concentration dependence of the corrected diffusivity [47].

$$D = D_o.\frac{d\ln p}{d\ln w}\bigg|_T \qquad (10)$$

Dawoud et al. [49], applied the Darken-corrected micro-pore diffusion coefficient to model the adsorption kinetics of water vapour into a consolidated DDZ-70 zeolite layer, achieving a very good agreement between the experimental data and the simulation results. The temperature dependence of the corrected diffusivity D_o is described in equation (11) by an Arrhenius relationship as a function of the parameters D_∞ and E_a along with the absolute adsorbent temperature.

$$D_o = D_\infty.\exp\left(-\frac{E_a}{R_m.T}\right) \qquad (11)$$

If the vapour velocity and, correspondingly, the pressure losses throughout the adsorbent bed are relatively low, the Darcy's law can be applied instead of the momentum conservation equation [50]. The Darcy's law (12) describes the velocity of the vapour as a viscous flow through the porous medium.
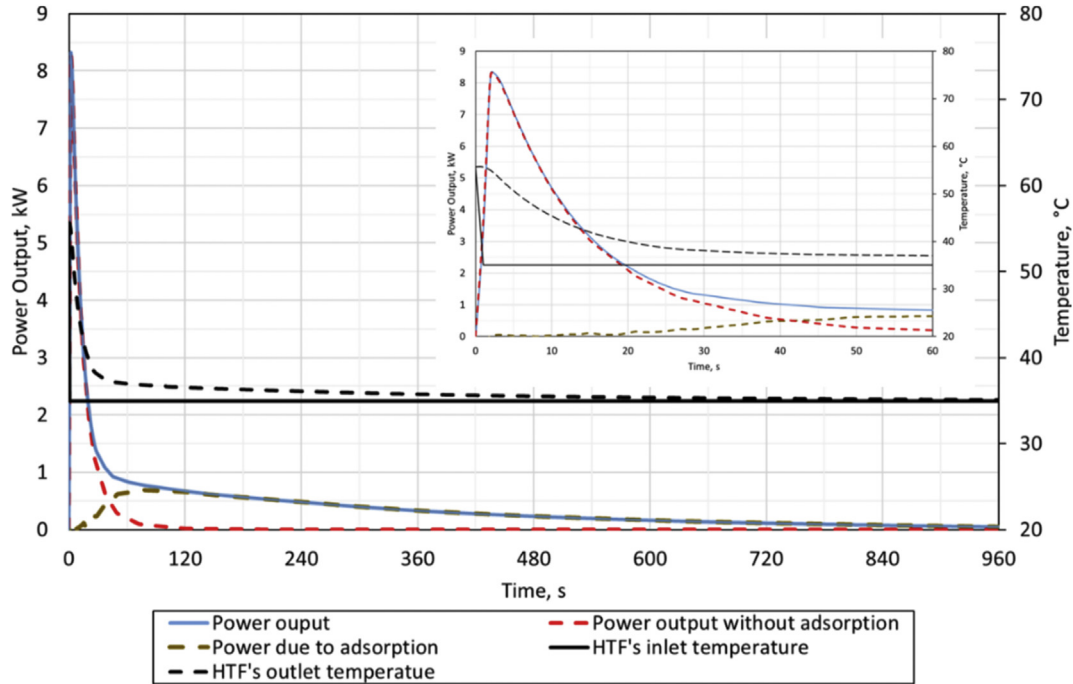
Fig. 7. APHE's power output and the contribution of the sensible heat stored in it along with the inlet and outlet temperatures of the HTF at the evaporator temperature of 5 °C and HTF's flow rate of 6 LPM.
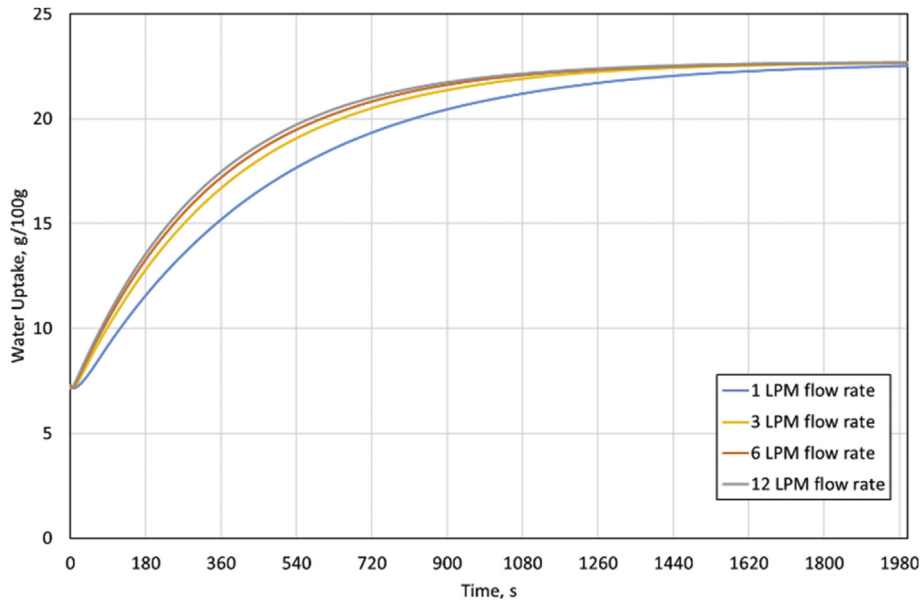
Fig. 8. Average water uptake dynamics of the introduced APHE at the evaporator temperature of 5 °C and different HTF's flow rates.

$$\overrightarrow{u_v} = -\frac{K_{app}}{\mu} \cdot \nabla p \tag{12}$$

where K_{app} is the permeability of the bed, which can be estimated according to equation (13), which has been introduced by Ruthven [45].

$$K_{app} = \frac{\varepsilon_b^3 d_p^2}{150(1 - \varepsilon_b)^2} \tag{13}$$

Beside the previously described equations for the combined heat and mass transfer encountered in the adsorbent sample tested in the kinetic setup, the following energy and momentum conservation equations for the APHE's metal and HTF domains are adopted for the 3-D mathematical model developed to simulate the representative intermediate domains of the proposed APHE.
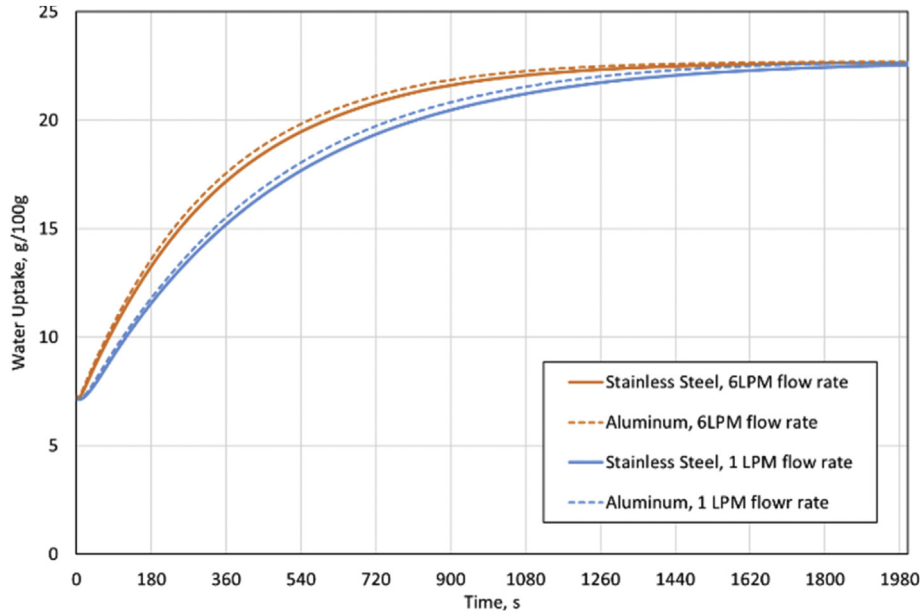
Fig. 9. Numerical water uptake dynamics of the introduced APHE with different construction materials at evaporator temperature of 5 °C and different HTF's flow rate.

Energy balance for the APHE's metal:

$$\rho_m C_m \frac{\partial T}{\partial t} + \nabla(-k_m \nabla T) = 0 \qquad (14)$$

where C_m and k_m are the heat capacity and the thermal conductivity of the metal, respectively.

Energy balance for the HTF:

The energy balance for the heat transfer fluid (HTF) is described by equation (15), from which the instantaneous temperature distribution along the APHE can be estimated.

$$\rho_f C_{p_f} \frac{\partial T}{\partial t} + \nabla\left(-k_f \nabla T\right) = -\nabla\left(\rho_f C_{p_f} \overrightarrow{u_f}\, T\right) \qquad (15)$$

Herein, C_{p_f} and k_f are the specific heat capacity and the thermal conductivity of the HTF, respectively. The $\overrightarrow{u_f}$ is the HTF's velocity vector. The HTF is assumed to be water, which has a relatively low thermal conductivity ($k_f = 0.59\ W^{-1}.m^{-1}.K^{-1}$). Therefore, heat transfer in the HTF is dominated by convection rather than conduction.

Momentum balance for the HTF:

The following momentum conservation equation accounts for the HTF's velocity distribution along the APHE. The flow regime inside the narrow flow channels of the introduced APHE is laminar. The following momentum (16) and mass conservation (17) equations are applied [51].

$$\rho_f \frac{\partial u_f}{\partial t} + \rho_f\left(u_f.\nabla\right)u_f = \nabla.\left[-pl + \mu\left(\nabla u_f + \left(\nabla u_f\right)^T\right) - \frac{2}{3}\mu\left(\nabla.u_f\right)l\right] + F \qquad (16)$$

$$\frac{\partial \rho_f}{\partial t} + \nabla.\left(\rho_f u_f\right) = 0 \qquad (17)$$

4.5. Initial conditions

The pressure, temperature, and adsorbate uptake distributions inside the experimentally tested adsorbent sample in the kinetic setup as well as the adsorbent domain of the proposed APHE are considered uniform at the initial state. The initial pressure of the water vapour inside the adsorbent is the saturation pressure corresponding to applied evaporator temperature. The initial temperature of the adsorbent is the corresponding adsorption start temperature ($T_{ad\text{-}start}$), which has been determined to 56 and 61 °C for the evaporator temperatures of 5 and 10 °C, respectively.

For the metal and HTF domains of the selected domains for simulating the APHE, a uniform temperature distribution of $T_{ad\text{-}start}$ is assumed at the initial state.

4.6. Boundary conditions

For the numerical simulation of the experimentally tested adsorbent sample, the instantaneously recorded temperature of the sample holder and the pressure of the water vapour inside the measuring cell are utilized as the related boundary conditions for the adsorbent domain. Since the frame, where the sample is placed inside, allows the vapour to enter only from one side, the experimentally recorded pressure variation inside the measuring cell is applied as the boundary condition at the sample vapour inlet, while zero normal pressure gradient $\left(\frac{\partial P}{\partial n} = 0\right)$ is assumed on all other boundaries. Moreover, the sample holder temperature recorded during the experimental work, from $T_{ad\text{-}start}$ to $T_{ad\text{-}end}$, is applied as the boundary condition at the lower surface of the adsorbent sample. For the other sides, insulation boundary conditions are applied ($\frac{\partial T}{\partial n} = 0$).

For the selected domains to simulate the APHE, symmetric heat and mass transfer boundary conditions ($\frac{\partial T}{\partial n} = 0$ and $\frac{\partial P}{\partial n} = 0$) are applied at the symmetry planes described before. In addition, insulation boundary conditions ($\frac{\partial T}{\partial n} = 0$) are applied at all outer sides of the adsorbent and metal domains. Different HTF-flow rates ($\dot{V}_{total}$) have been considered. At the HTF's inlet port, fully

developed flow with flow rate of $\frac{\dot{V}_{total}}{4\,N_{plate-pairs}}$ and temperature of T_{ad-end} is assumed.

4.7. Implementation

The commercial COMSOL Multiphysics® code, which employs the transient finite element multi-dimensional modelling, is applied for all simulation tasks. First, a 2-D geometry representative for the experimentally investigated adsorbent sample is implemented. The adsorbent domain is treated as a porous media. The physical properties of AQSOA-Z02/water pair required for the simulation work are taken from Refs. [36,52]. The "heat transfer in porous medium" module integrated in COMSOL is applied to account for the energy conservation. The "Darcy's law" module is applied to account for the inter-particle mass transfer resistance. The "chemical reaction" module is employed to represent the linear driving force (LDF) model, which accounts for the intra-particle diffusion resistance. The integrated optimization module is applied to estimate the parameters of the diffusion coefficient of water vapour into the zeolite pellets by best fitting the experimental results obtained by the kinetic setup.

Afterwards, a 3-D geometry for the selected domains of the APHE is implemented in COMSOL Multiphysics®. The "conjugate heat transfer" module integrated in COMSOL Multiphysics® is applied instead of the "heat transfer in porous medium" module to account for the heat transfer on the three contacted domains; namely the porous medium of the adsorbent, the metal and the HTF domains. The main advantage of applying this module is that there is no need to define convective heat transfer coefficients at the contact surfaces between the related domains [53]. The other modules applied in the simulation of adsorbent sample are applied also to account for the mass transfer in the tested adsorbent domain of the selected adsorbent domains of the APHE. The estimated values of D_∞ and E_a are fed to the "chemical reaction" module to account for the mass diffusion resistance in the adsorbent grains. In addition, the integrated "laminar flow" module is applied to account for the momentum conservation in the HTF.

The effect of the grid size and number of elements on the accuracy of the simulation results has been carefully investigated. To this aim, the number of grid elements has been changed from 265,601 to 2,136,471. It turned out, that a grid of 744,293 elements was adequate to obtain grid-independent results. The model has been solved in transient mode for 2000 s with a variant time step between 0.01 and 0.1 s. The relative tolerance has been set to 1e−3.

5. Results

In this section, the adsorption kinetic results, obtained experimentally are presented and compared with some literature values. Moreover, the values estimated for the D_∞ and E_a by best fitting the obtained experimental data with numerical results using COMSOL's optimization module are discussed. Finally, the results obtained from the 3D model developed to simulate the representative domains of the APHE are presented and thoroughly discussed.

5.1. The representative adsorbent sample

Fig. 4 presents the experimentally obtained water uptake at evaporator temperatures of 5 and 10 °C starting at a water uptake of 7 g/100 g, which corresponds to a desorption temperature of 90 °C and a condenser temperature of 35 °C. The adsorption start temperatures amount to 56 and 61 °C for the evaporator temperatures of 5 and 10 °C, respectively. For both measurements, the adsorption-end temperature is 35 °C. Based on the individual

uncertainties of the applied measuring sensors listed in Table 1, the maximum error associated with measuring the temporal differential water uptake is estimated to ±0.332 and ± 0.36 g/100 g in case of the adsorption at the evaporator temperature of 5 and 10 °C, respectively. The continuous lines depict the simulated adsorption kinetics of the tested sample by the 2-D model. The best fitting between both experimental and simulated kinetic results has been achieved with a micro-pore diffusion coefficient at infinite temperature (D_∞) of 2 E−4 (m^2s^{-1}) and an activation energy of 42.1 (kJ mol^{-1}).

These values are very close to those of water vapour adsorption in silica gel obtained in Ref. [40,54]. Such an agreement between the effective water vapour diffusivities in silica gel and zeolite pellets has been reported on by Riffel et al. [55], who developed a transient mathematical model to simulate the performance of an adsorber heat exchanger. To account for the mass transfer, they used the definition of the time lag or the time constant (τ) instead of the diffusion coefficient. Strictly speaking, Riffel et al. [55] has applied the following equation to describe the mass transfer or the time rate of pressure change inside the pores of the adsorbent grains (dp/dt) as a function of the temporal pressure difference between the vapour phase of the adsorber chamber (P_{ch}) and inside the adsorbent grains (p)

$$\frac{dP}{dt} = \frac{1}{\tau}(P_{ch} - P) \tag{18}$$

By R^2-maximisation (coefficient of multiple determination), the time constants that best fit the model to the dynamic measurements of water vapour adsorption on silica gel and zeolite AQSOA-Z02 were estimated to τ = 151.7 s for both adsorbents.

Fig. 5 illustrates, in addition, the results obtained previously by Dawoud [21] upon investigating the adsorption kinetics of two different coated adsorber heat exchangers made of aluminium, which has been operated against a stagnant pool evaporator inside an adsorption heat pump module. The first adsorber heat exchanger was a finned flat-tube heat exchanger (FFT) made of brazed aluminium, while the second was an extruded-tube aluminium heat exchanger (ET). The numbers given aside to the abbreviations (ET or FFT) in Fig. 4 correspond to the layer thickness in μm of the coated AQSOA-Z02 layers by Mitsubishi Plastic Incorporation. All five heat exchangers were investigated under evaporator, condenser and adsorber-end temperatures of 5 and 35 °C, respectively, while the desorption temperature amounted to 90 °C. This allows the direct comparison with the results obtained at 5 °C evaporator temperature for the representative test segment of the introduced APHE. From the heat capacity ratio point of view and, correspondingly, the COP point of view, the extruded tube aluminium heat exchanger coated with 500 μm (ET500) is comparable with the introduced APHE. The achieved differential water uptake with the introduced APHE at 300 and 600 s amount to 8.2 and 12.2 g/100 g, respectively. This corresponds to a remarkable enhancement of 310% (compared to 2 g/100 g) and 165% (compared to 4.6 g/100 g) at 300 and 600 s if compared with the ET500 adsorber heat exchanger. The obtained results pave the way to step to the next development phase, namely to fabricate and investigate the APHE under different operating conditions of heat transformation processes.

5.2. Simulation results of the APHE

The values estimated before for D_∞ and E_a have been applied in the 3D simulations. Fig. 5 illustrates a good agreement between the water uptake obtained from the numerical simulation of the APHE and that obtained from the experimental investigation of the

representative segment depicted in Fig. 2 at the evaporator temperatures of 5 and 10 °C.

The small deviation between the experimental and the numerical results is attributed to the applied boundary conditions (constant pressure for the APHE versus reduced pressure on the V-LTJ-kinetic measurements) and the accuracy of the AQSOA-Z02/water pair's equilibrium model, which is responsible for the small deviation in the final equilibrium uptake. Beside the thickness and the width of the space provided for placing the adsorbent material in the APHE, which are responsible for the mass transfer dynamics, a quick thermal response of the surface temperature of the plates to the sudden change in HTF's inlet temperature is also necessary to obtain sound combined heat and mass transfer characteristics from the adsorber heat exchanger. In order to achieve the later requirement, a uniform flow distribution of the HTF over all plate-pairs and inside each plate over all flow channels shall be guaranteed. In addition, the sum of the thermal capacities of the metal and the HTF of APHE related to the thermal capacity of the adsorbent must be minimized. The distribution of the HTF flow over the plate pairs and, in each, over the flow channels guarantees a low pressure loss and consequently a low parasitic energy consumption of the circulation pumps. Due to the low hydraulic diameter of the flow channels, a high convective heat transfer coefficient is realized, despite the resulted laminar flow regime.

Fig. 6 presents the change in the measured temperature of the sample holder's surface of the kinetic setup (Fig. 2-b) and the numerical average surface temperature of one APHE plate, after the sudden change of the HTF's inlet temperature. In the experimental work, the sample holder temperature starts to decrease once the sample holder is connected to the thermal circulating bath set at $T_{ads-end}$. This is done by changing the position of the three way valves connecting the sample holder with the thermal circulating baths [34,35].

As shown in Fig. 6 the rate of temperature decrease of both the surface of the sample holder and APHE's plates is almost identical over the first 20 s, after which the temperature is reduced to 38 °C. In the remaining time, the further reduction to 35 °C is faster in the kinetic setup as the sample mass is very low (250 mg) compared to the adsorbent mass on the adsorbent domain of the APHE. The comparison depicted in Fig. 6 implies that the dynamic performance measured with the representative segment of the APHE is very much applicable to the dynamic performance of the real APHE.

5.3. Adsorber power output

Fig. 7 illustrates the numerically estimated power output of the introduced APHE, which consists of 24 plate pairs offering an adsorbent volume of 1 L or 700 g AQSOA-Z02 at an evaporator temperature of 5 °C and a HTF flow rate of 6 LPM. Because of the simulated large temperature jump isobaric adsorption phase, the temporal adsorber power increases sharply and reaches up to 8.25 kW during the first few seconds. This is attributed to the step change in the HTF's inlet temperature. At the time of peak power, the HTF's outlet temperature is still very close to the APHE's initial temperature (56 °C), whereas the inlet temperature attains the adsorprion-end temperature ($T_{ad-end} = 35$ °C). Afterwards, the power output decreases rapidly and gets lower than 3 kW after 15 s. After that time, the adsorber power continues to decrease, but with a clearly slower rate until it reaches almost zero power after 960 s. In order to evaluate the relative values of both sensible and adsorption heat amounts, a dedicated simulation run has been carried out without allowing the adsorption process to take place. The power associated with removing the sensible heat stored in the APHE's material, HTF and the adsorbent, is presented by the dashed red line, which vanishes almost completely after 2 min. The

solid blue line represents the overall power including that due to the release of the heat of adsorption. By subtracting the sensible heat related power (dashed red line) from the overall measured power (solid blue line), the power due to the release of the heat of adsorption has been evaluated and presented by the dashed brown line. The cross over between both contributions (cross point between both dashed red and green lines) takes place after 42 s from the beginning of the adsorption process and, from there on, the release and removal of the heat of adsorption dominates the process dynamics.

As explained before, the lower the sensible heat stored in the metal and the HTF of the adsorber HX compared to the stored heat of adsorption, the higher the COP of the adsorption system. From the specific power (SP) point of view, this sensible heat has to be rapidly transferred to the HTF to allow a rapid and effective cooling of the adsorbent material and, consequently, a fast adsorption process leading to a high cooling capacity. The integration of the area under the curve of the power due to the release of the heat of adsorption or the integration of the area between the two power curves (with and without adsorption), over the process' time equals the released heat of adsorption. This concept has been introduced by Tokarev and Aristov [56] to estimate the temporal development of the uptake upon experimentally testing representative pieces of adsorber heat exchangers.

5.4. Effect of the HTF's flow rate

Fig. 8 depicts the effect of the flow rate of the HTF on the adsorption kinetics. Increasing the flow rate of the HTF leads to enhancing the convective heat transfer coefficient on the HTF side. The overall heat transfer coefficient is dominated, however, by the heat transfer on the adsorbent side, due to its very low thermal conductivity. Increasing the HTF's flow rate above 3 l/min (LPM) for the encountered 24 plate pairs, is obviously not leading to a remarkable enhancement in the adsorption dynamics, compared to the dynamics increase between 1 and 3 LPM.

5.5. Effect of the construction material

The proposed APHE is decided to be made of stainless steel (SS) in order to completely avoid any corrosion potential against water or ethanol as refrigerants [57] or the application of selective water sorbents, which is formed by impregnating hygroscopic salts like LiBr or LiCl [8−10] inside the pores of mesoporous adsorbents. Fig. 9 depicts the adsorption kinetics obtained numerically from the APHE's simulation at an evaporator temperature of 5 °C and the HTF flow rates of 1 and 6 LPM for both aluminium and SS as construction materials. According to the presented results, the construction material has a very limited effect on the performance of the introduced APHE. Among other factors, the adsorption dynamics of the APHE depend on the relative magnitudes of the thermal diffusivities of the construction material and the adsorbent. The thermal diffusivity of SS amounts to 3.8×10^{-06} [m^2/s], which is 18 times higher than the thermal diffusivity of the adsorbent (FAM-Z02). This implies that the dynamics of adsorption is dedicated by the thermal diffusivity inside the adsorbent domain. The improvement of the thermal diffusivity of the construction material by making use of aluminium is, therefore, not leading to a remarkable enhancement on the adsorption dynamics.

6. Conclusion

An innovative plate heat exchanger is developed and introduced to act as a durable and high efficient adsorber in adsorption heat transformation processes like chillers, heat pumps as well as heat

and cold storage. First experimental investigations on the adsorption dynamics of the introduced APHE have been carried out on a representative test frame, which has been constructed to simulate the heat and mass transfer characteristics of the introduced APHE. Experimental adsorption kinetic measurements on a small-scale adsorbent sample inside the test frame have been carried out at two different evaporator temperatures in a V-LTJ kinetic setup at OTH Regensburg University.

In addition, a transient 2-D mathematical model is developed to simulate the combined heat and mass transfer encountered in the investigated adsorbent sample. The model has been implemented in a commercial simulation software and its optimization module has been utilized to estimate the diffusion parameters. This methodology resulted in a mico-pore diffusion coefficient at infinite temperature (D_∞) of 2×10^{-04} $[m^2 s^{-1}]$ and an activation energy of 42.1 $[kJ\ mol^{-1}]$. The mathematical model is further developed to simulate the introduced APHE. To this aim, a 3-D geometry comprising 3 domains, HTF, metal and the adsorbent/adsorbate is implemented in the commercial simulation software, which makes use of the obtained D_∞ and E_a from the previous activities. The results obtained from the investigation of the adsorbent sample demonstrated the superiority of the introduced APHE over an extruded aluminium heat exchanger coated with a 500 μm layer of the same adsorbent. Comparing the obtained results with the literature values for the extruded aluminium heat exchanger, differential water uptake obtained after 300 s of adsorption (8.2 g/100 g) implies a sound enhancement of 310%. This result proves the great potential of the introduced APHE to enhance remarkably the performance of adsorption heat transformation appliances.

Credit author statement

On the Development of an Innovative Adsorber Plate Heat Exchanger for Adsorption Heat Transformation Processes; An Experimental and Numerical Study Makram Mikhaeil: Conceptualization, Model, Investigation, Validation, Writing - original draft Matthias Gaderer: Supervision, Writing- Reviewing and Editing Belal Dawoud: Funding acquisition, Project administration, Supervision, Conceptualization, Methodology, Formal analysis, Writing-Reviewing and Editing

Declaration of competing interest

The authors declare that they have no known competing financial interests or personal relationships that could have appeared to influence the work reported in this paper.

Acknowledgements

References

[1] Langan M, O'Toole K. A new technology for cost effective low grade waste heat recovery. Energy Procedia 2017;123:188–95.
[2] Wang LW, Wang RZ, Wu JY, Xu YX, Wang SG. Design, simulation and performance of a waste heat driven adsorption ice maker for fishing boat. Energy 2006;31(2–3):244–59.
[3] Miyazaki T, Akisawa A. The influence of heat exchanger parameters on the optimum cycle time of adsorption chillers. Appl Therm Eng 2009;29(13):2708–17.
[4] Verde M, Cortés L, Corberán JM, Sapienza A, Vasta S, Restuccia G. Appl Therm Eng 2010;30(13):1511–22.
[5] Sapienza A, Santamaria S, Frazzica A, Freni A. Influence of the management strategy and operating conditions on the performance of an adsorption chiller. Energy 2011;36(9):5532–8.
[6] El Fadar A. Novel process for performance enhancement of a solar continuous adsorption cooling system. Energy 2016;114:10–23.
[7] Yeboah SK, Darkwa J. A critical review of thermal enhancement of packed beds for water vapour adsorption. Renew Sustain Energy Rev 2016;58:1500–20.
[8] Aristov Y, et al. Selective water sorbents for multiple applications. React Kinet Catal Lett 1996;59:325–34.
[9] Aristov Y e al. New family of materials for adsorption cooling: material scientist approach. J Eng Thermophys 2007;16:63–72.
[10] Aristov Y. Challenging offers of material science for adsorption heat transformation: a review. Appl Therm Eng 2013;50(2):1610–8.
[11] Cabeza LF, Sole A, Barreneche C. Review on sorption materials & technologies for heat pumps and thermal energy storage. Renew Energy 2017;110:3–39.
[12] Gordeeva LG, Aristov YI. Adsorptive heat storage and amplification: new cycles and adsorbents. Energy 2019;167:440–53.
[13] Jeremias F, Khutia A, Henninger SK, Janiak C. MIL-100(Al, Fe) as water adsorbents for heat transformation purposes—A promising application. J Mater Chem 2012;22:10148–51.
[14] Zhou HC, Long JR, Yaghi OM. Introduction to metal–organic frameworks. Chem Rev 2012;112:673–4.
[15] Saha BB, El-Sharkawy II, Miyazaki T, Koyama S, Henninger SK, Herbst A, Janiak C. Ethanol adsorption onto metal organic framework: theory and experiments. Energy 2015;79:363–70.
[16] de Lange MF, van Velzen BL, Ottevanger CP, Verouden KJ, Lin LC, Vlugt TJ, Gascon J, Kapteijn F. Metal–organic frameworks in adsorption–driven heat pumps: the potential of alcohols as working fluids. Langmuir 2015;31:12783–96.
[17] Saha BB, Uddin K, Pal A, Thu K. Emerging sorption pairs for heat pump applications: an overview. JMST Advances 2019;4:1–20.
[18] Freni A, Dawoud B, Bonaccorsi L, Chmielewski S, Frazzica A, Calabrese L, Restuccia G. Springer briefs in applied sciences and technology. Springer; 2015. ISBN 978-3-319-09326-0.
[19] Bendix P, Füldner G, Möllers M, Kummer H, Schnabel L, Henninger S, Henning HM. Optimization of power density and metal-to-adsorbent weight ratio in coated adsorbers for adsorptive heat transformation applications. Appl Therm Eng 2017;124:83–90.
[20] Lang R, Roth M, Stricker M, Westerfeld T. Development of a modular zeolite-water heat pump. Heat Mass Tran 1999;35(3):229–34.
[21] Dawoud B. Water vapour adsorption kinetics on small and full scale zeolite coated adsorbers; A comparison. Appl Therm Eng 2013;50(2):1645–51.
[22] Aristov YI, Glaznev IS, Girnik IS. Optimization of adsorption dynamics in adsorptive chillers: loose grains configuration. Energy 2012;46(1):484–92.
[23] Bonaccorsi L, Proverbio E. Synth. of thick zeolite 4A coatings on stainless steel. Microporous Mesoporous Mater 2004;74:221–9.
[24] K Okamoto, et al. Development of AQSOA water adsorbent and coated heat exchanger. In: IMPRES Conference 7-32.
[25] Waszkiewicz SD, Tierney MJ, Scott HS. Development of coated, annular fins for adsorption chillers. Appl Therm Eng 2009;29(11–12):2222–7.
[26] Freni A, et al. SAPO-34 coated adsorbent heat exchanger for adsorption chillers. Appl Therm Eng 2015;82:1–7.
[27] Sapienza A, et al. Effect of residual gas on dynamics of isobaric adsorption of a chiller. Appl Therm Eng 2016;96:385–90.
[28] Rogala Z. Adsorption chiller using flat-tube adsorbers—Performance assessment and optimization. Appl Therm Eng 2017;121:431–42.
[29] Sharafian A, Bahrami M. Assessment of adsorber bed designs in waste-heat driven adsorption cooling systems for vehicle air conditioning and refrigeration. Renew Sustain Energy Rev 2014;30:440–51.
[30] Gordeeva L, Frazzica A, Sapienza A, Aristov Y, Freni A. Adsorption cooling utilizing the "LiBr/silica–ethanol" working pair: dynamic optimization of the adsorber/heat exchanger unit. Energy 2014;75:390–9.
[31] Golparvar B, Niazmand H, Sharafian A, Hosseini AA. Optimum fin spacing of finned tube adsorber bed heat exchangers in an exhaust gas-driven adsorption cooling system. Appl Energy 2018;232:504–16.
[32] Palomba V, Dawoud B, Sapienza A, Vasta S, Frazzica A. On the impact of different management strategies on the performance of a two-bed activated carbon/ethanol refrigerator: an experimental study. Energy Convers Manag 2017;142:322–33.
[33] Dawoud B. European patent application. 2018. EP 3 382 313 A1, 03.10.
[34] Aristov YI, Dawoud B, Glaznev IS, Elyas A. A new methodology of studying the dynamics of water sorption/desorption under real operating conditions of adsorption heat pumps: experiment. Int J Heat Mass Tran 2008;51(19–20):4966–72.
[35] Dawoud B. On the effect of grain size on the kinetics of water vapor adsorption and desorption into/from loose pellets of FAM-Z02 under a typical operating condition of adsorption heat pumps. J Chem Eng Jpn 2007;40(13):1298–306.
[36] Frazzica A, Freni A. Adsorbent working pairs for solar thermal energy storage in buildings. Renew Energy 2017;110:87–94.
[37] Intini M, Goldsworthy M, White S, Joppolo CM. Experimental analysis and numerical modelling of an AQSOA zeolite desiccant wheel. Appl Therm Eng 2015;80:20–30.
[38] Yamamoto T, Kim YH, Kim BC, Endo A, Thongprachan N, Ohmori T. Adsorption characteristics of zeolites for dehydration of ethanol: evaluation of diffusivity of water in porous structure. Chem Eng J 2012;181:443–8.
[39] Ali SM, Chakraborty A. Thermodynamic modelling and performance study of

an engine waste heat driven adsorption cooling for automotive air-conditioning. Appl Therm Eng 2015;90:54−63.

[40] Chihara K, Suzuki M. Air drying by pressure swing adsorption. J Chem Eng Jpn 1983;16(4):293−9.

[41] Youssef PG, Mahmoud SM, Al-Dadah RK. Performance analysis of four-bed adsorption water desalination/refrigeration system, comparison of AQSOA-Z02 to silica-gel. Desalination 2015;375:100−7.

[42] Teo HWB, Chakraborty A, Fan W. Improved adsorption characteristics data for AQSOA types zeolites and water systems under static and dynamic conditions. Microporous Mesoporous Mater 2017;242:109−17.

[43] Pesaran A, Lee H, Hwang Y, Radermacher R, Chun HH. Numerical simulation of adsorption heat pumps. Energy 2016;100:310−20.

[44] Chua HT, Ng KC, Wang W, Yap C, Wang XL. Transient modeling of a two-bed silica gel−water adsorption chiller. Int J Heat Mass Tran 2004;47(4):659−69.

[45] Ruthven DM. Principles of adsorption and adsorption processes. John Wiley & Sons; 1984.

[46] Sakoda A, Suzuki M. Fundamental study on solar powered adsorption cooling system. J Chem Eng Jpn 1984;17(1):52−7.

[47] Karger J, Ruthven DM. Diflusion in zeolites. Handbook of zeolite science and technology 1992:341−423.

[48] Darken LS. Diffusion, mobility and their interrelation through free energy in binary metallic systems. Trans. Aime 1948;175:184−201.

[49] Dawoud B, Vedder U, Amer EH, Dunne S. Non-isothermal adsorption kinetics of water vapour into a consolidated zeolite layer. Int J Heat Mass Tran 2007;50(11−12):2190−9.

[50] Ellis MW. An evaluation of the effect of adsorbent properties on the performance of a solid sorption heat pump. PhD Thesis. Georgia Institute of Technology; 1996.

[51] Peric M. A finite volume method for the prediction of three-dimensional fluid flow in complex ducts. PhD Thesis. University of London; 1985.

[52] Charalambous C, Santori G, Vilarrasa-Garcia E, Bastos-Neto M, Cavalcante Jr CL, Brandani S. Pure and binary adsorption of carbon dioxide and nitrogen on AQSOA FAM Z02. J Chem Eng Data 2018;63(3):661−70.

[53] Radu AI, Defraeye T, Ruch P, Carmeliet J, Derome D. Insights from modeling dynamics of water sorption in spherical particles for adsorption heat pumps. Int J Heat Mass Tran 2017;105:326−37.

[54] Aristov YI, Tokarev MM, Freni A, Glaznev IS, Restuccia G. Kinetics of water adsorption on silica Fuji Davison RD. Microporous Mesoporous Mater 2006;96(1−3):65−71.

[55] Riffel DB, Wittstadt U, Schmidt FP, Nunez T, Belo FA, Leite AP, Ziegler F. Transient modeling of an adsorber using finned-tube heat exchanger. Int J Heat Mass Tran 2010;53(7−8):1473−82.

[56] Tokarev MM, Aristov YI. A new version of the Large Temperature Jump method: the thermal response (T−LTJ). Energy 2017;140:481−7.

[57] Proverbio E, Calabrese L, Caprì A, Bonaccorsi L, Dawoud B, Frazzica A. Susceptibility to corrosion of aluminium alloy components in ethanol adsorption chiller. Renew Energy 2017;110:174−9.